Cement and Concrete Research 40 (2010) 415–425

Contents lists available at ScienceDirect

Cement and Concrete Research

journal homepage: http://ees.elsevier.com/CEMCON/default.asp

Concrete cover cracking with reinforcement corrosion of RC beam during chloride-induced corrosion process

Ruijin Zhang [a,*], Arnaud Castel [b], Raoul François [b]

[a] Modern Design and Analysis Research Institute, Northeastern University, Shenyang, China
[b] LMDC (Laboratoire Matériaux et Durabilité des Constructions), Université de Toulouse, UPS, INSA, Toulouse, France

ARTICLE INFO

Article history:
Received 17 April 2009
Accepted 29 September 2009

Keywords:
Crack detection (B)
Corrosion (C)
Reinforcement (D)
Concrete (E)
Modeling (E)

ABSTRACT

This paper deals with the evolution of the corrosion pattern based on two beams corroded by 14 years (beam B1CL1) and 23 years (beam B2CL1) of conservation in a chloride environment. The experimental results indicate that, at the cracking initiation stage and the first stage of cracking propagation, localized corrosion due to chloride ingress is the predominant corrosion pattern and pitting corrosion is the main factor that influences the cracking process. As corrosion cracking increases, general corrosion develops rapidly and gradually becomes predominant in the second stage of cracking propagation. A comparison between existing models and experimental results illustrates that, although Vidal et al.'s model can better predict the reinforcement corrosion of beam B1CL1 under localized corrosion, it cannot predict the corrosion of beam B2CL1 under general corrosion. Also, Rodriguez's model, derived from the general corrosion due to electrically accelerated corrosion experiments, cannot match natural chloride corrosion irrespective of whether corrosion is localized or general. Thus, for natural general corrosion in the second stage of cracking propagation, a new model based on the parameter of average steel cross-section loss is put forward to predict steel corrosion from corrosion cracking.

1. Introduction

One of the main causes of premature damage in reinforced concrete structures is reinforcement corrosion. Accurate information on corrosion distribution along the reinforcement is the basis of mechanical behaviour analysis of corroded elements. As an important characteristic of corrosion, the longitudinal cracks provide a visual sign of reinforcement corrosion within concrete. Damage can be detected visually because the coincident cracks along the reinforcement are related with both the reduction of the rebar cross-section and the loss of bond between reinforcement and concrete. This provides a possible approach for non-destructive evaluation of the corrosion state of reinforcement.

Although there are several methods for non-destructively studying the evolution of corrosion, such as electrochemical techniques [1–3], radar measurements, etc. [4], it is impossible to accurately assess the corrosion distribution along reinforcements embedded in concrete. Therefore, some experimental work based on accelerated tests or the natural corrosion process has been carried out in order to study the empirical link between the occurrence and widths of cracks and the amount of corrosion products. As the corrosion process due to electrically accelerated tests is very different from natural corrosion, the works by Alonso et al. [5] and Rodriguez et al. [6] may not be representative of the real on-site situation. In contrast, Vidal et al. [7] studied two 3-m-long beams corroded in an aggressive saline environment and subjected to wetting–drying cycles and sustained loading. Although the wetting–drying cycles were used to accelerate the corrosion process, the corrosion distribution, corrosion type and the oxides produced were very much closer to those of natural chloride-induced corrosion than those resulting from the use of an electrical current or a $CaCl_2$ admixture in the concrete [8].

In this paper, the evolution of the corrosion pattern due to chloride ingress is firstly discussed on the basis of cracking maps and the real corrosion distributions along reinforcements of two corroded beams, B1CL1 and B2CL1, that had been exposed to a chloride environment for 14 years and 23 years respectively. Then, existing models derived from accelerated corrosion or natural corrosion are compared with the experimental results to clarify the influence of corrosion pattern evolution and the relation between accelerated corrosion and natural corrosion. A new model, based on experimental results under a general corrosion pattern, is put forward to predict reinforcement corrosion from corrosion crack width.

2. Experimental programme

2.1. Reinforced concrete specimens

The reinforced concrete specimens studied in this paper were cast in 1984 in order to study the steel corrosion process and its influence

* Corresponding author.
E-mail address: rjzhang@mail.neu.edu.cn (R. Zhang).

0008-8846/$ – see front matter © 2009 Elsevier Ltd. All rights reserved.
doi:10.1016/j.cemconres.2009.09.026

on the mechanical behaviour of reinforced concrete elements [9–12]. The full-size beams (300×28×15 cm) were stored in an aggressive environment under loading. The layout of reinforced concrete beams is shown in Fig. 1. The aggressive environment was a salt fog (35 g/l of NaCl corresponding to the chloride concentration of sea water). All the beams were loaded in 3-point bending. Two loading values were used: Mser1 = 13.5 kNm (beams labelled B1CL or A1CL) or Mser2 = 21.2 kNm (beams labelled B2CL or A2CL). More details on this long-term experimental programme are available in [12].

The concrete mix and the cement chemical composition are given in Tables 1 and 2. Water content was adjusted to obtain a slump of 7 cm. The average compressive strength and elastic modulus obtained on cylindrical specimens (110×220 mm) were 45 MPa and 32 GPa at 28 days.

2.2. Cracking map

After 14 and 23 years of exposure, a large number of longitudinal cracks due to reinforcement corrosion could be observed on all the surfaces of the corroded beams. Prior to the destructive experiment on the corroded beams, their cracking maps were drawn with the locations of flexural transverse cracks and longitudinal corrosion cracks. Only the widths of longitudinal corrosion cracks were indicated on the maps. The crack widths were measured using a binocular lens with an accuracy of 0.02 mm.

2.3. Corrosion distribution

To evaluate the corrosion damage, the covering concrete was completely removed from the reinforcement. The steel cross-section reductions were assessed from the reinforcement mass loss. Using the parts of the same rebar in non-corroded areas as the reference mass of reinforcement per unit of length, the residual mass per unit of length of the sample in corroded areas was evaluated after complete removal of the corrosion products (using Clark's solution ANSI/ASTM G1-72) and then related to the reference mass. The average reinforcement mass loss Δm per unit of length was then calculated. In the case of local pitting attacks, the length of the samples could be less than 5 mm. The steel cross-section loss was finally deduced from the loss of mass using Eq. (1):

$$\Delta A_s = \frac{\Delta m}{m} \cdot A_s \tag{1}$$

where ΔA_s is the average steel cross-section loss (mm^2) over the sample length, A_s is the sound steel cross-section (mm^2) and m is the reference mass per unit of length.

Table 1
Concrete composition (kg/m^3).

Mix component		
Rolled gravel (silica + limestone)	5/15 mm	1220
Sand	0/5 mm	820
Portland cement: OPC HP (high perform)		400
Water		200

3. Experimental results

3.1. Cracking maps

The cracking maps of the corroded beam are presented in Fig. 2 for B1CL1 after 14 years of exposure and in Fig. 3 for B2CL1 after 23 years of exposure. Flexural transversal cracks resulting from three-point-flexure had appeared in the tensile central part of the beam where the stresses in the concrete exceeded its tensile strength.

For beam B1CL1 after a period of 14 years (Fig. 2), only four corrosion cracks were randomly distributed along the reinforcement in the compressive zone. Their widths were less than 0.5 mm. In contrast, the corrosion cracks in the tensile zone were more concentrated in the middle part, especially around the mid-span of the back surface, where the crack widths had reached 1.4 mm.

For beam B2CL1 after a period of 23 years (Fig. 3), the cracks in the compressive zone were longer and wider than those of beam B1CL1, with the maximum crack width reaching 2.8 mm. The locations of cracks were also irregular. In the tensile zone, the corrosion cracks on

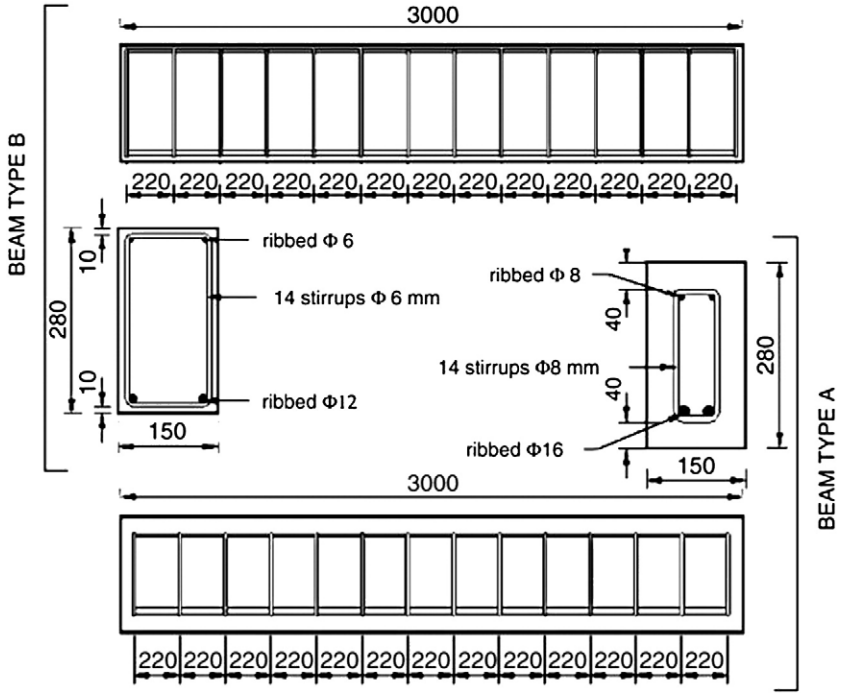

Fig. 1. Layout of the reinforced concrete beams (all dimensions in mm).

Table 2
Cement composition (%).

	SiO_2	Al_2O_3	Fe_2O_3	CaO	MgO	SO_3	Na_2O
Weight	21.4	6.0	2.3	63.0	1.4	3.0	0.5

the tensile surface had developed and interconnected, with crack widths reaching more than 3 mm at mid-span. Several independent cracks were found on the front and back surfaces along the tensile steel bars.

3.2. Distribution of reinforcement cross-section loss

Along the reinforcements of B1CL1 and B2CL1, red and brownish-red coloured rusts were observed in different amounts and at various positions on the steel bar surfaces. Even on the same reinforcement, the corrosion activities were also different depending on the locations along the rebar. It was obvious that the steel bars of B2CL1 were more corroded than those of B1CL1.

Figs. 4 and 5 show the corrosion of tensile rebars and compressive rebars respectively of corroded beam B1CL1. For the tensile rebars, the maximum cross-section reduction occurred on the back tensile rebar around the mid-span (Fig. 4). In the central zone, more or less general corrosion could be observed along corrosion cracks but the localized pitting corrosion was still relatively predominant (Fig. 6 (a)). In addition, several isolated pitting attacks were found along the bars outside the central part. Around these pitting attacks corresponding to corrosion cracks less than 0.5 mm wide, no obvious general corrosion was found (Fig. 6 (b)). For the compressive rebars (Fig. 5), the corrosion activity was randomly distributed in agreement with the locations of corrosion cracks on the beam surfaces.

The corrosion distributions of the reinforcements of B2CL1 are shown in Figs. 7 and 8. Along the tensile rebars (Fig. 7), the corrosion developed more extensively than that of B1CL1 (Fig. 4) and the general corrosion became the predominant pattern although some pitting attacks could be easily distinguished (Fig. 9). Corrosion occurred homogeneously around the cross-section of the steel bars. Along the compressive bars of B2CL1 (Fig. 8), the corrosion distribution was similar to that of B1CL1, with higher losses of cross-section and larger crack widths. In the non-cracked region, several pitting attacks and slight general corrosion were detected on the lower half surface of the steel according to the casting direction, where voids had formed due to the effect of bleeding. Other researchers have observed the same phenomenon [13,14].

It should be pointed out that the reinforcing steel bars located in the vicinity of the stirrups were always less corroded than the adjacent parts of the same rebar (Figs. 7 and 10). In fact, the stirrup locations always corresponded to the occurrence of flexural cracks. The short-term experimental results (5 years) showed that corrosion only started at the tips of flexural cracks [8]. But the long-term experimental results reported here are clearly in agreement with the conclusions of other researchers and show that flexural cracks did not significantly influence the long-term corrosion process of tensile bars and corrosion cracking [12,15,16]. Corrosion at flexural transverse crack tips only concerned the lower part of the stirrups and did not affect the structural performance. The combined effects of crack self-healing due to concrete re-hydration and healing due to the free expansion of corrosion products along these cracks, led to a negligible corrosion rate in the long term.

4. Corrosion pattern evolution

Although the pitting attack is an important characteristic of chloride-induced corrosion, the experimental results obtained on beams B1CL1 and B2CL1 showed that the corrosion pattern evolved towards the general corrosion pattern with the development of cracking during the natural corrosion process. The evolution of the corrosion pattern versus time is schematically shown in Fig. 11.

4.1. Corrosion initiation

At the beginning of the experiment, the flexural cracks resulting from three-point-flexure encouraged corrosion to occur firstly on the steel located at the flexural crack tip (after only a few months). This corrosion activity slowed down and stopped due to self-healing phenomena [16–18]. At this stage, no corrosion cracks appeared.

Afterwards, the chloride ions penetrated through the concrete and reached the threshold value (about 0.4% per cement mass) at the depth of the steel rebars. Along the rebars, localized breakdown of the passive

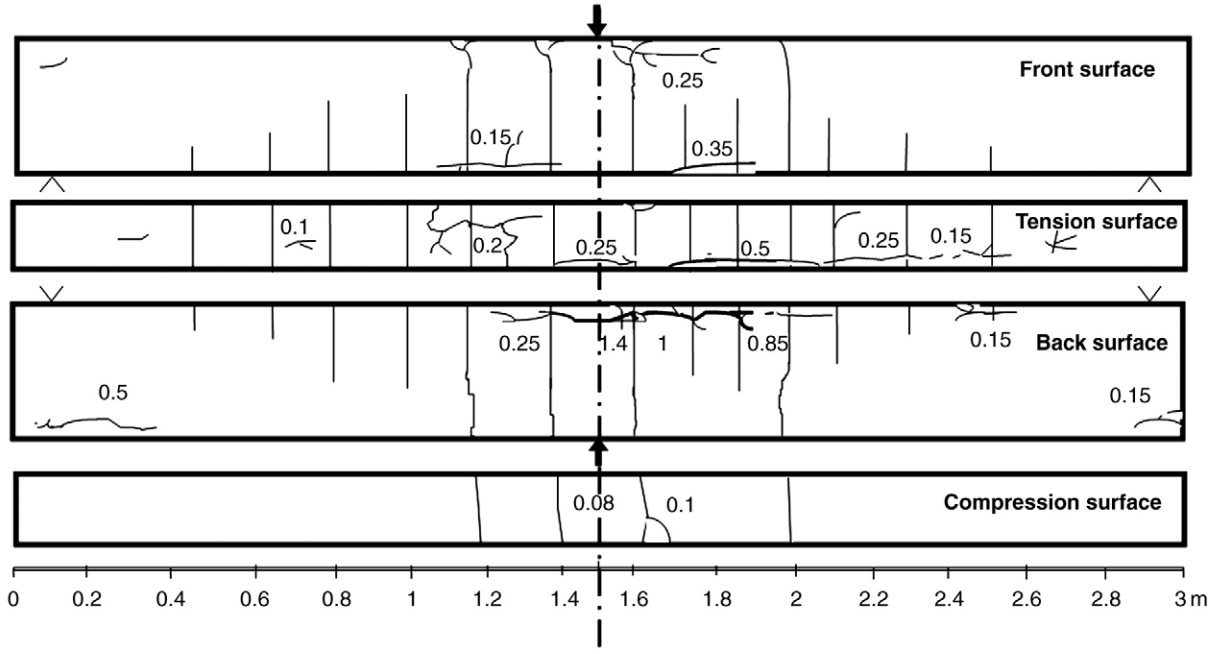

Fig. 2. Cracking maps of beam B1CL1 at 14 years.

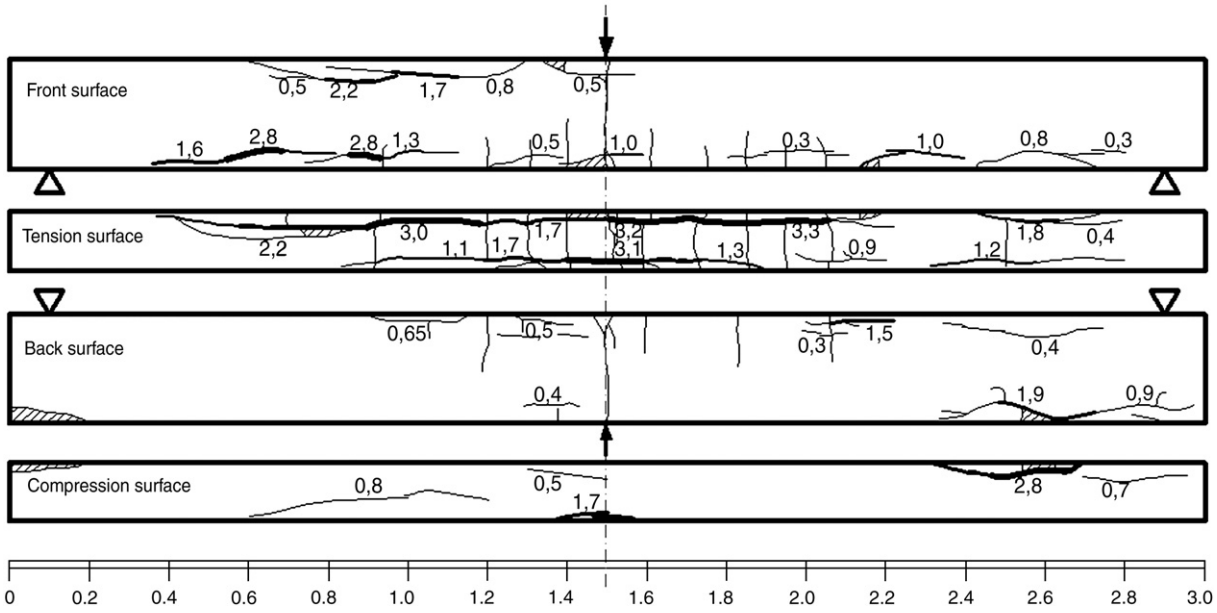

Fig. 3. Cracking maps of beam B2CL1 at 23 years (the hatched parts represent concrete that has fallen off).

film due to chloride ingress occurred randomly at the locations of imperfect passive film and interface defects [19]. This led to the initiation of pitting corrosion.

4.2. Cracking initiation

Corrosion products are expansive and have greater volume than the initial steel. This induces corrosion cracking when the resulting tensile stress in the surrounding concrete reaches the tensile strength limit of concrete. Therefore, during this period, localized corrosion due to chloride ingress is the main corrosion pattern. This is consistent with the observation of the steel bars of beam B1CL1 after 14 years of exposure. Localized corrosion was still the prominent pattern along beam B1CL1 except in the central part where the corrosion cracks were already quite wide after 14 years in a chloride environment (Figs. 4 and 5).

4.3. First stage of cracking propagation

Corrosion cracking leads to the deterioration of the steel–concrete interface along a significant length of the steel bars. The aggressive agents can reach the steel surface more easily as corrosion cracking develops. Thus, more or less general corrosion was observed along the corrosion cracks of beam B1CL1 in the central part (Fig. 6 (A)). The pattern here was different from that in other locations with smaller corrosion crack widths (Fig. 6 (B)). However, at the beginning of corrosion cracking, the corrosion cracks are always short and very narrow, which limits the access of aggressive agents to the steel bars. So general corrosion progresses very slowly and pitting attacks still remain predominant, as observed on most of the corroded beam B1CL1 (Figs. 4 and 5). In this period, the small, independent corrosion cracks should depend on the maximum localized pitting corrosion within the region of the crack.

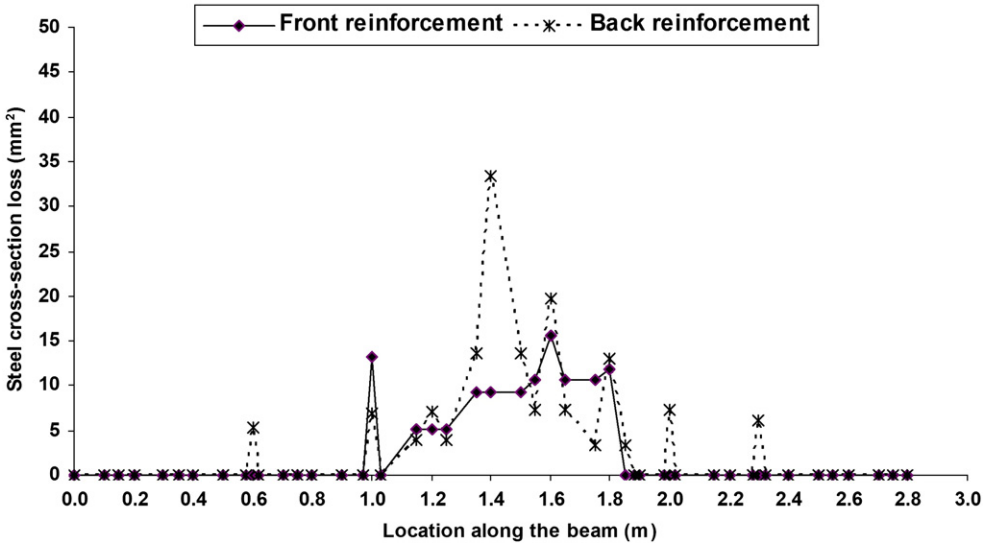

Fig. 4. Distribution of corrosion along the tensile reinforcements of beam B1CL1.

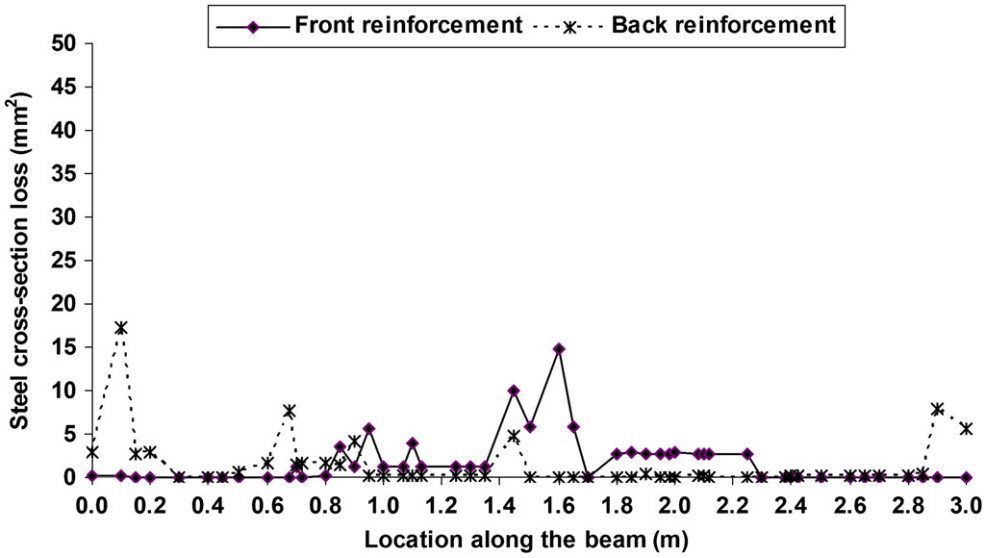

Fig. 5. Distribution of corrosion along the compressive reinforcements of beam B1CL1.

4.4. Second stage of cracking propagation

In this stage, as corrosion develops, the longitudinal corrosion cracks interconnect and grow wider. This leads to further steel–concrete interface degradation and exposes more steel surface to chloride, humidity and oxygen. Hence, in these areas, general corrosion develops and gradually becomes predominant. This corrosion pattern could be observed on the tensile reinforcements of B2CL1 after 23 years of exposure (Figs. 9–10). Although some pitting attacks deeper than nearby general corrosion still existed, the beam B2CL1 obviously corresponded to the second stage of cracking propagation as general corrosion was distributed along almost all the central part (Fig. 7).

In conclusion, the occurrence of corrosion cracks and their widening modify the corrosion pattern along the steel reinforcing bars. In fact, reinforcement corrosion distributions in large-dimension concrete elements are complex and develop gradually. It is difficult to accurately ascertain the division between the first stage and the second stage of cracking propagation. However, in the first stage, corrosion cracks resulting from localized pitting corrosion are always short and independent on the surfaces of beam whereas, in the second stage, corrosion cracks interconnect and widen along the rebars. Research of Poupard et al. [20] on a RC beam after 40 years natural exposure in marine environment shows that the high corrosion zones close to the corrosion induced cracks have a different morphology of corrosion products in comparison with the low corrosion zones. Therefore, when we study the correlation between corrosion cracking and reinforcement corrosion, it is necessary to take into account the evolution of the corrosion pattern during the corrosion process.

5. Comparison between experimental results and existing models

To assess reinforcement corrosion from corrosion cracks, some researchers have proposed models based on the attack penetration parameter [5,6], while others have proposed models based on the cross-section loss of steel rebar [7]. In this section, two existing models, one derived from natural corrosion and the other from accelerated corrosion experimental results, will be introduced. The models were tested using the experimental results obtained on the corroded beams corresponding to different corrosion phases to clarify the influence of corrosion pattern.

5.1. Determination of equivalent crack width

For one location of reinforcement corrosion, cracking can be observed on one surface or two surfaces around the rebar (Fig. 12). So the equivalent crack width corresponding to the same corroded area

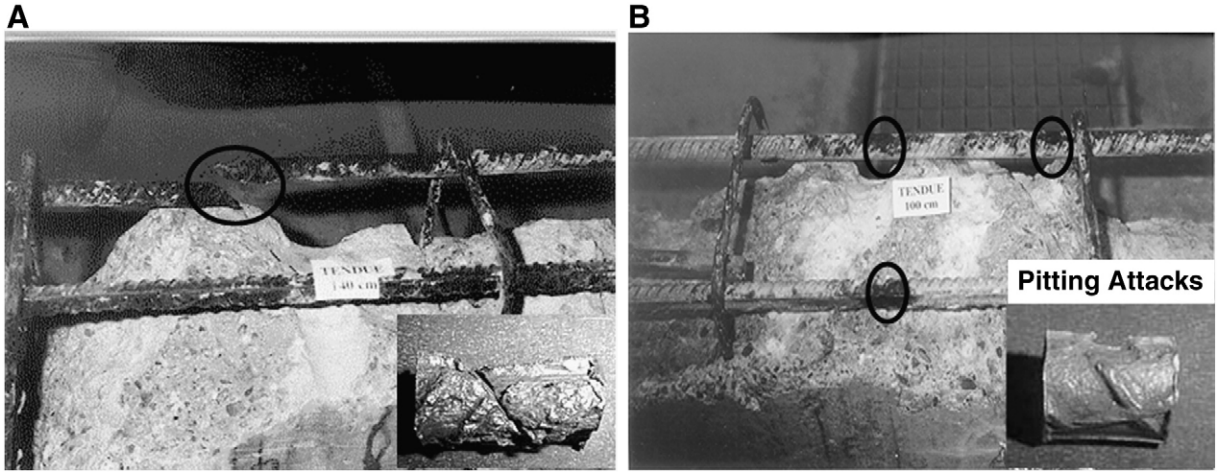

Fig. 6. Corrosion on the tensile steel bars of beam B1CL1 at 14 years. (A) Central zone. (B) Pitting attacks.

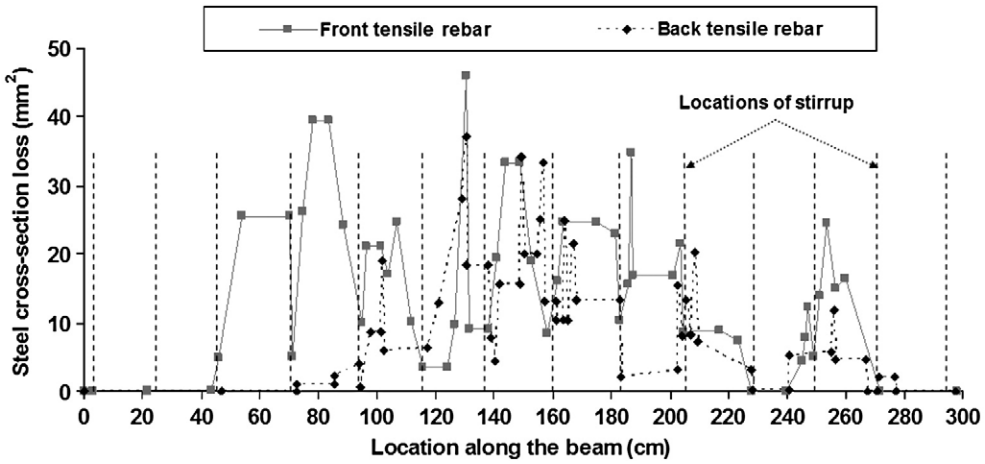

Fig. 7. Distribution of corrosion along the tensile reinforcements of beam B2CL1.

should consider the crack widths on the two beam surfaces. For case 1, the equivalent width w_{eq} is the sum of both cracks w_1 and w_2. For case 2, the equivalent width w_{eq} is the width of one crack w_3.

5.2. Vidal et al.'s model linking corrosion crack width to local cross-section reduction

Vidal et al.'s model [7] predicts the local cross-section loss of reinforcement from the crack width following two steps of the cracking process: cracking initiation and cracking propagation.

5.2.1. Steel cross-section loss initiating cracking

In the cracking initiation period, corrosion products have to firstly fill in the local pores and deposit at the steel–concrete interface before they generate radial pressure on the surrounding concrete. The steel cross-section loss ΔA_{s0} due to localized corrosion necessary for cracking initiation can be calculated using Eq. (2):

$$\Delta A_{s0} = A_s\left[1-\left[1-\frac{\alpha}{\phi_0}\left(7.53+9.32\frac{c}{\phi_0}\right)10^{-3}\right]^2\right] \quad (2)$$

where, ΔA_{s0} is the steel cross-section loss for cracking initiation (mm^2), A_s is the sound steel cross-section (mm^2), ϕ_0 is the initial reinforcement diameter (mm), c is the covercrete (mm), and α is the pit penetration parameter: $\alpha=2$, for homogeneous corrosion and $4<\alpha<8$, for localized corrosion [6].

This equation does not take the concrete characteristics into account (concrete tensile strength, porosity, etc.) because Vidal et al.'s model is derived from experimental data obtained from beams cast with the same concrete, which is also the concrete used for the beams considered in this paper.

5.2.2. Relationship between crack width and local steel cross-section loss

According to Vidal et al.'s model, during the cracking propagation phase, the crack width is directly linked to the volume of oxides, which is proportional to the steel cross-section loss. A linear relationship linking the local reinforcement cross-section loss to the crack width is proposed in [7]. The empirical linear expression predicting crack propagation is as follows:

$$w = K(\Delta A_s - \Delta A_{s0}) \quad (3)$$

where, w is the crack width (mm), ΔA_s is the local steel cross-section loss (mm^2), $K=0.0575$, and $r^2=0.82$ (from the regression).

Vidal et al.'s model was derived from the experimental results obtained on two corroded beams B1CL1 and A1CL1 exposed for 14 years and 17 years respectively.

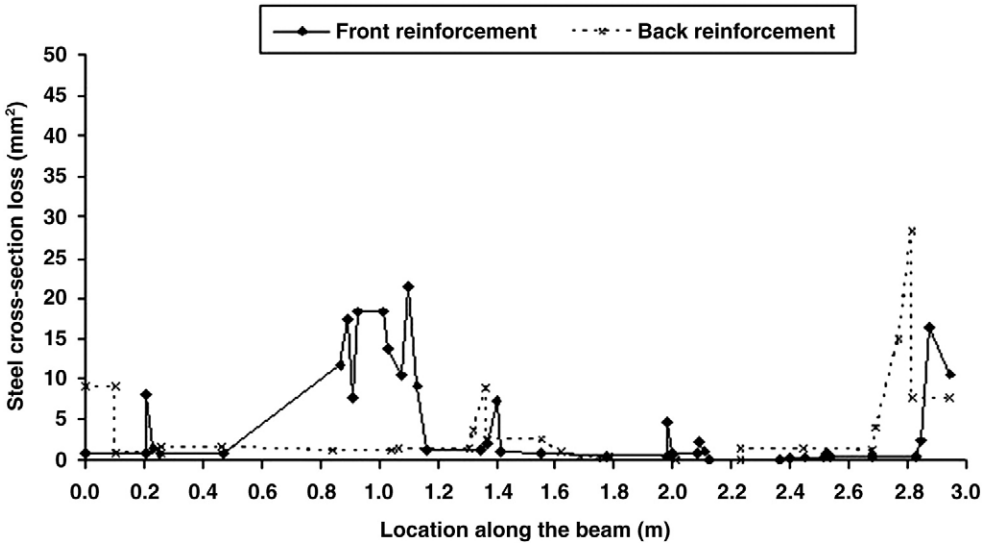

Fig. 8. Distribution of corrosion along the compressive reinforcements of beam B2CL1.

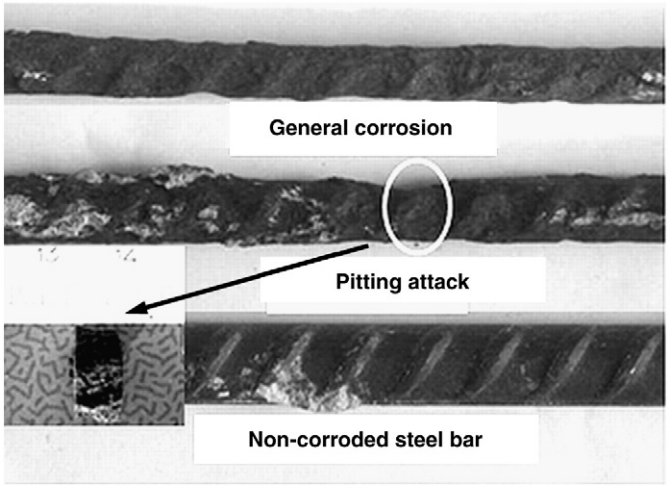

Fig. 9. Corrosion on the tensile steel bars of beam B2CL1 in the central zone at 23 years.

5.3. Rodriguez's model linking corrosion crack width to attack penetration

According to Rodriguez et al. [6], attack penetration can be calculated from the measured loss of steel mass using Eq. (4), which presents the relationship between corrosion (pitting attack or homogeneous corrosion) and reinforcement diameter decrease (Fig. 13):

$$\phi = \phi_0 - \alpha x \tag{4}$$

where, ϕ is the residual bar diameter; ϕ_0 is the initial bar diameter; x is the attack penetration; α is the attack penetration parameter: $\alpha=2$, for homogeneous corrosion; $4<\alpha<8$, for localized corrosion.

The relationship between corrosion attack penetration and the steel cross-section loss Eq. (5) can be deduced by combining Eqs. (1) and (4):

$$x = \frac{\phi_0}{\alpha}\left[1-\sqrt{1-\frac{\Delta A_s}{A_s}}\right]10^3 \tag{5}$$

where, x is the attack penetration (μm), ϕ_0 is the initial bar diameter (mm), ΔA_s is the steel cross-section loss (mm^2), and A_s is sound steel cross-section (mm^2).

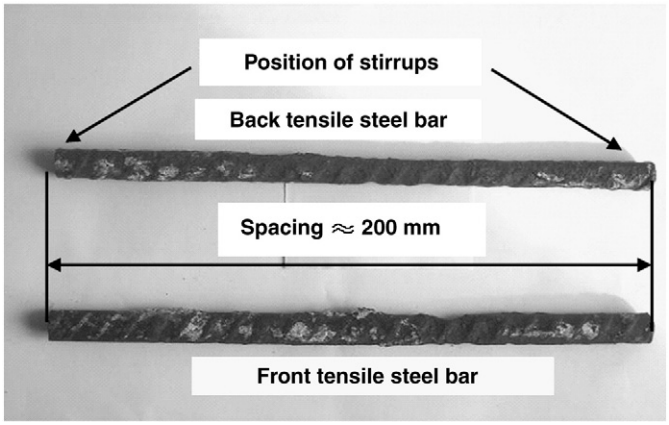

Fig. 10. The portions of tensile rebars between two stirrups of corroded beam B2CL1 at 23 years.

Eq. (5) shows that, for the same initial rebar diameter ϕ_0 and the same cross-section loss ΔA_s, homogeneous corrosion or pitting attack can lead to very different attack penetration values.

To link the steel corrosion to cracking evolution, a linear relationship Eq. (6) proposed by Alonso et al. [5] predicts the attack penetration required for corrosion cracking initiation.

$$x_0 = 7.53 + 9.32\frac{c}{\phi_0} \tag{6}$$

where, x_0 is the attack penetration needed to initiate cracking (μm).

During the cracking propagation phase, a general form of the linear relation between crack width and attack penetration proposed by Rodriguez et al. [6] is:

$$w = 0.05 + \beta(x - x_0) \tag{7}$$

where, x is the attack penetration (μm) and β is the coefficient depending on the position of rebar: $\beta=0.01$ for top cast bar; $\beta=0.0125$ for bottom cast bar.

However, the reinforcement position considered by the model of Rodriguez (coefficient β) seems to have no influence on cracking development, because the voids under the upper bar with respect to the casting direction will only delay cracking initiation. In other words, the steel bar's position only affects the value of attack penetration that initiates cracking. Thus, for reinforcements at different positions, Eq. (7) should have the same slope but with different intercepts corresponding to the attack penetration values necessary for cracking initiation, which depend on the concrete characteristics, concrete cover and initial rebar diameter as well as the position of the rebar.

Below, the Rodriguez model of beam B was obtained as Eq. (7a) by applying the parameters of tensile reinforcement of beam B in Eqs. (6) and (7).

$$\text{For beam B}: w = 0.0125x - 0.1995. \tag{7a}$$

5.4. Comparison between experimental results and existing models

Fig. 14 shows the predictions of existing models and the experimental results obtained on corroded beam B1CL1 after 14 years of exposure, beam A1CL1 after 17 years and beam B2CL1 after 23 years. All details for beam A1CL1 are available in [7]. The predominant pitting attacks of beams A1CL1 and B1CL1 show that both of them were situated in the localized corrosion pattern stage (Fig. 6). Their experimental results were obtained by sampling the steel bars, adjusting the size of samples to the pit size. Each sample included one pit of corrosion. In contrast, the extensive general corrosion along the tensile reinforcements of B2CL1 showed that the beam corresponded to the general corrosion pattern stage. For beam B2CL1, the experimental results were obtained in two steps. Firstly, the steel bars were divided into several portions of about 200 mm length (Fig. 10) cut at the locations of the stirrups, which corresponded to relatively low steel cross-section loss. Each portion was considered as an individual sample, the mass loss of which was weighed to calculate the average cross-section loss (Fig. 15). Secondly, the portions of corroded rebar were divided into much smaller samples to obtain detailed information on corrosion distribution (Fig. 7).

In Fig. 14, for consistency with Vidal et al.'s model based on the local pitting pattern, the maximum steel cross-section reduction corresponding to the maximum width of crack in each portion of beam B2CL1was chosen as an experimental point (Fig. 15). Depending on the locations of the portions along the reinforcement, this maximum steel section loss could correspond to local pitting attacks or uniform corrosion values. Vidal et al.'s model and Rodriguez's model are also presented in Fig. 14. Rodriguez's model with $\alpha=8$ corresponds to

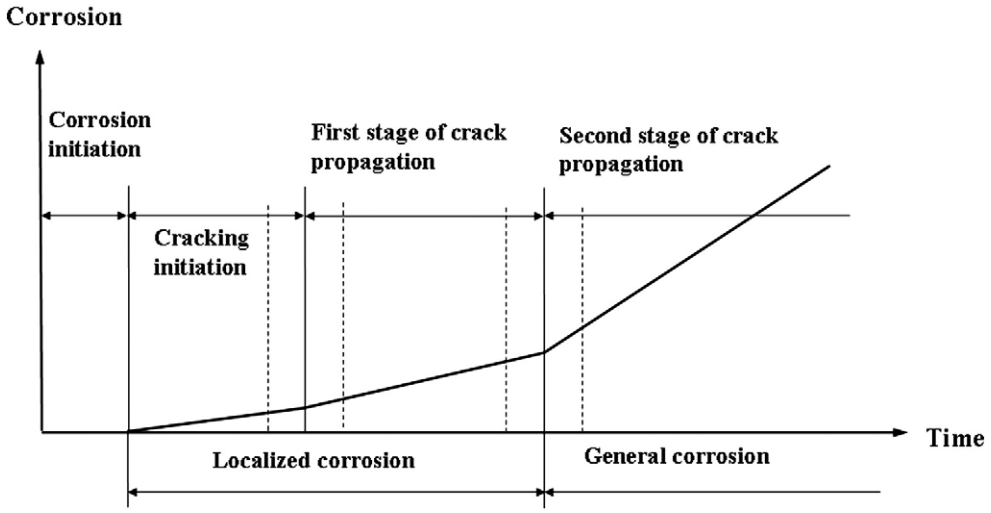

Fig. 11. Corrosion pattern evolution versus time under natural chloride-induced corrosion.

pitting attack, and Rodriguez's model with $\alpha=2$ corresponds to homogeneous corrosion at the cross-section of the steel bar (Fig. 13).

It is obvious that only the points of beams B1CL1 and A1CL1 exhibit an acceptable correlation with the linear relationship of Vidal et al.'s model. This can be attributed to the reinforcements of both beams being in the first stage of cracking propagation even though low general corrosion had occurred in the central zone of the tensile reinforcements of B1CL1. Most longitudinal corrosion cracks along tensile reinforcements were small, and the reinforcement corrosion thus appeared as discontinuous pitting attacks and non-symmetric corrosion at the steel cross-section (Fig. 6). Consequently, the corrosion cracking width was only related to the maximum localized corrosion within the region of the crack. Nevertheless, the predictions of Rodriguez's model ($\alpha=8$), which corresponds to pitting attack (Fig. 13), slightly underestimate the reinforcement corrosion in the localized corrosion stage. This can be explained by the fact that the corrosion accelerated by electrical currents is much closer to a general corrosion, which is different from the localized corrosion induced by natural chloride attack. Although a penetration parameter α was adopted to represent the difference in the two corrosion patterns, Rodriguez's model based on accelerated corrosion still deviated from the natural experimental results.

However, Vidal et al.'s model was significantly conservative for the experimental results of corroded beam B2CL1 (Fig. 14); almost all the experimental points lay above the prediction line of the model. In fact, after 23 years of exposure, beam B2CL1 was already in the second stage of cracking propagation, with large, interconnected longitudinal cracks, and predominance of the general corrosion pattern (Fig. 9). Comparing the curve of cracking width with the reinforcement corrosion distribution (Fig. 15) clearly showed that the cracking width was no longer correlated with the maximum steel cross-section loss. The maximum value of 46 mm^2 for local steel cross-section loss corresponds to a crack width of 2.5 mm at the central zone of the front tensile rebar. Thus, in the second stage of cracking propagation, the crack width at one location did not only depend on the local cross-section reduction at the same location but was also affected by the surrounding general corrosion and the extension of nearby large corrosion cracks. This can explain why the experimental results of B2CL1 were not reproduced by Vidal et al.'s model. On the other hand, although corrosion on the cross-section of the steel rebar was quite symmetric and approached homogeneity for B2CL1, Rodriguez's model with $\alpha=2$ corresponding to homogeneous corrosion still could not predict the reinforcement corrosion well (Fig. 14). The model evidently underestimates the reinforcement corrosion from the crack width and the experimental points lie below the model line. Thus general corrosion accelerated by electrical current does not represent the natural general corrosion pattern successfully.

In conclusion, due to the evolution of the corrosion pattern during the natural chloride corrosion process, the existing models only predict a part of the experimental results corresponding to the period

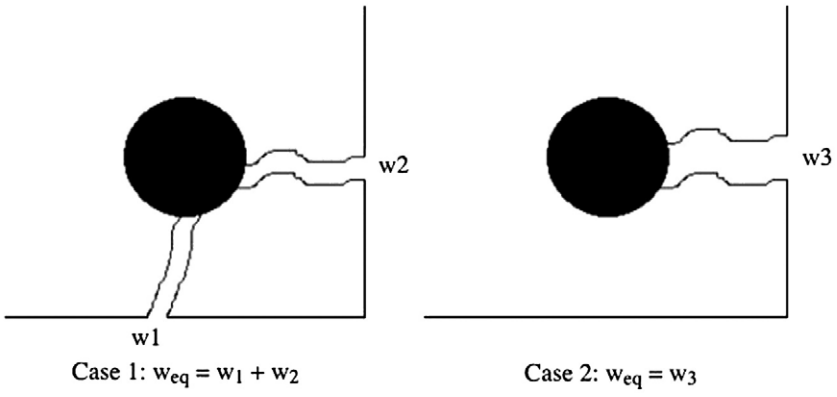

Fig. 12. Examples of equivalent crack configurations for a given corrosion state [7].

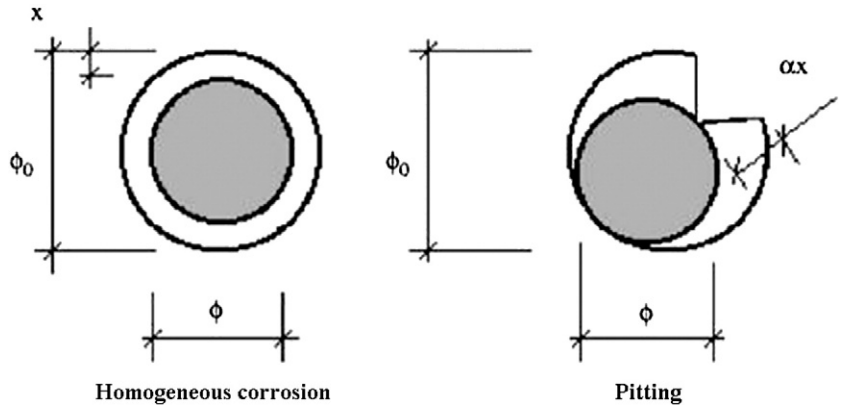

Fig. 13. Residual reinforcing bar section [6].

of cracking initiation and the first stage of cracking propagation, where localized corrosion is the predominant pattern. For the localized corrosion pattern stage, Vidal's model is better than Rodriguez's model for predicting the maximum local cross-section loss of the steel bar from the corrosion crack width. For the general corrosion pattern stage, it is necessary to propose a new relationship linking crack width to reinforcement corrosion.

It can be seen in Fig. 14 that the experimental points of B2CL1 show significant scatter in comparison with those of beams B1CL1 and A1CL1. This also can be attributed to the evolution of the corrosion pattern. As discussed above, for B1CL1 and A1CL1, the maximum local cross-section loss of reinforcement was obviously a suitable parameter to describe the cracking process in the first stage of cracking propagation while the localized corrosion was the predominant pattern. Nevertheless, for beam B2CL1 in the second stage of cracking propagation, in which the general corrosion became the predominant pattern, this parameter was no longer the main cause that influenced the evolution of corrosion cracks. Therefore, it is necessary to choose a new parameter to describe the reinforcement corrosion.

6. New model predicting the reinforcement corrosion based on the general corrosion pattern

Under the general corrosion pattern, the average cross-section loss parameter ΔA_{sm} was chosen rather than the local cross-section loss as the parameter to describe the reinforcement corrosion in the second stage of cracking propagation. As mentioned above, the tensile reinforcements of beam B2CL1 were firstly divided into several portions about 200 mm long according to the locations of the stirrups (Fig. 10). The average cross-section loss ΔA_{sm} of each portion was obtained by measuring its mass loss, Δm, and then using Eq. (1). The average cross-section loss was better correlated with the corrosion crack width than the local maximum cross-section loss for the front tensile reinforcements of beam B2CL1 (Fig. 15).

Fig. 16 shows the experimental results of average steel cross-section loss in relation to crack widths measured on two tensile reinforcements of beam B2CL1. The points are obviously correctly represented by a linear relationship. This confirms that the average steel cross-section loss is a more suitable parameter to describe the cracking propagation in the second stage of cracking propagation. The empirical linear expression predicting crack propagation under the general corrosion pattern is as follows:

$$w = 0.1916\Delta A_{sm} + 0.164 \tag{8}$$

where w is the crack width (mm), ΔA_{sm} is the average cross-section loss (mm^2), and $r^2 = 0.8572$ from the regression.

In comparison with the new proposed model, Rodriguez's model ($\alpha = 2$) presented in the same figure underestimates the steel corrosion: most of the experimental values of average cross-section

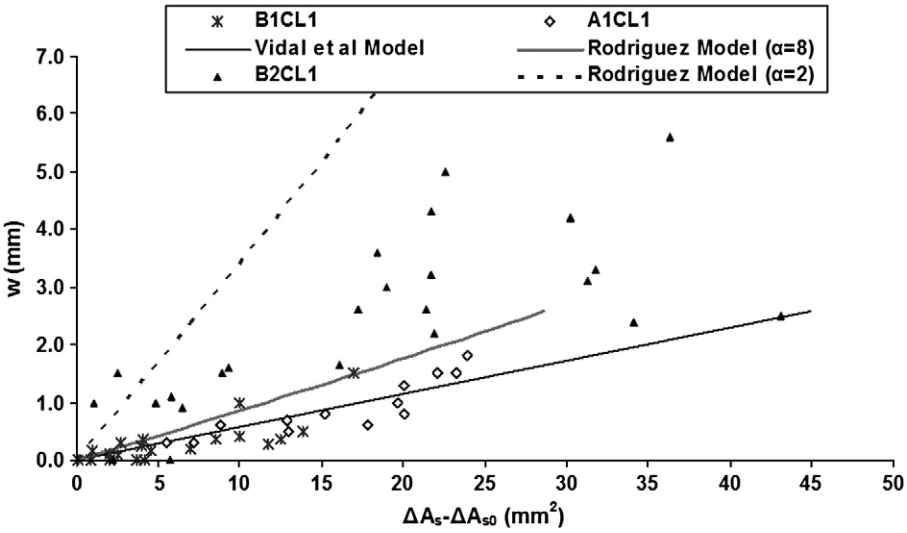

Fig. 14. Crack width evolution versus local steel cross-section loss of corroded beams.

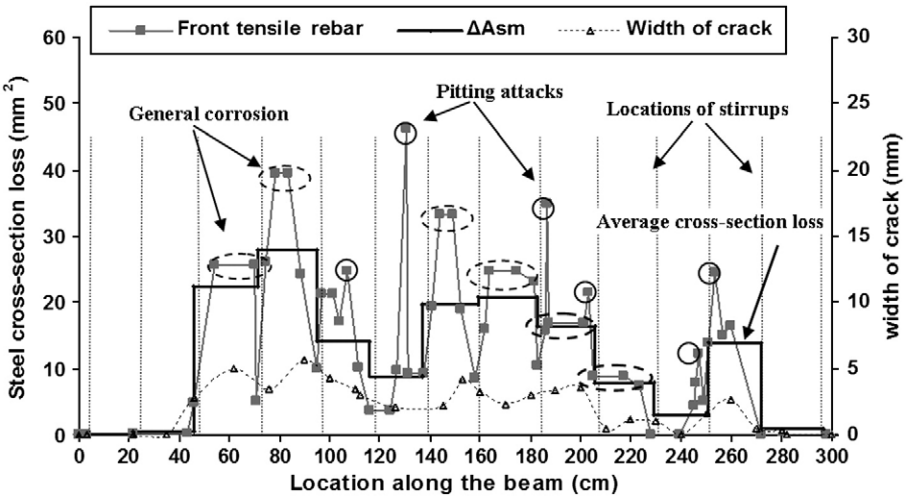

Fig. 15. Maximum local cross-section loss and average cross-section loss versus crack width measured on the front tensile reinforcement of beam B2CL1.

loss are greater than the predictions of the model. Therefore, although the corrosion morphology of accelerated corrosion is much closer to the general corrosion pattern, the deduced model does not match the experimental results obtained in the general corrosion pattern of natural chloride-induced corrosion.

As mentioned by Vidal et al. [7], this model does not take the concrete characteristics (concrete tensile strength, porosity, etc.) into account because all the beams used in this study were cast using the same concrete. Thus, the experimental data available do not allow any conclusions to be drawn on the influence of concrete characteristics. Moreover, it is not sure whether the concrete cover affects the relationship between general corrosion and crack width in the second stage of cracking propagation because the experimental data about general corrosion were only obtained on beam B2CL1. Therefore, the new proposed model should be further verified in situ or on other corroded elements.

7. Conclusion

Although the localized corrosion of pitting attacks is the only corrosion pattern at the beginning of natural chloride-induced corrosion, the corrosion pattern develops with the presence of corrosion cracking and cracking development. The corrosion cracking process should be divided into three phases in terms of corrosion pattern evolution and the relationship linking reinforcement corrosion with crack width within these phases is as follows:

- During the cracking initiation phase, the local pitting attack due to chloride ingress is the only corrosion pattern. The necessary localized section loss for cracking initiation ΔA_{s0} is calculated using Eq. (2) with $\alpha = 8$, which represents the pit penetration parameter of the localized corrosion pattern.
- During the first stage of cracking propagation, corrosion cracks are still independent along the reinforcements, and localized corrosion remains predominant. The pits of corrosion are discontinuous along the rebars and the corrosion is not symmetric on the steel cross-section. The crack width w is related to the maximum localized corrosion of reinforcement ΔA_s using Eq. (3).
- During the second stage of cracking propagation, wide corrosion cracks result in general corrosion along a large part of the reinforcements in front of the cracks. General corrosion becomes the predominant corrosion pattern and corrosion is much closer to homogeneous corrosion on the cross-section of steel. The quite continuous corrosion along steel rebars makes the average cross-section loss ΔA_{sm} the decisive parameter of crack width w. The width of crack w can be calculated using Eq. (8).

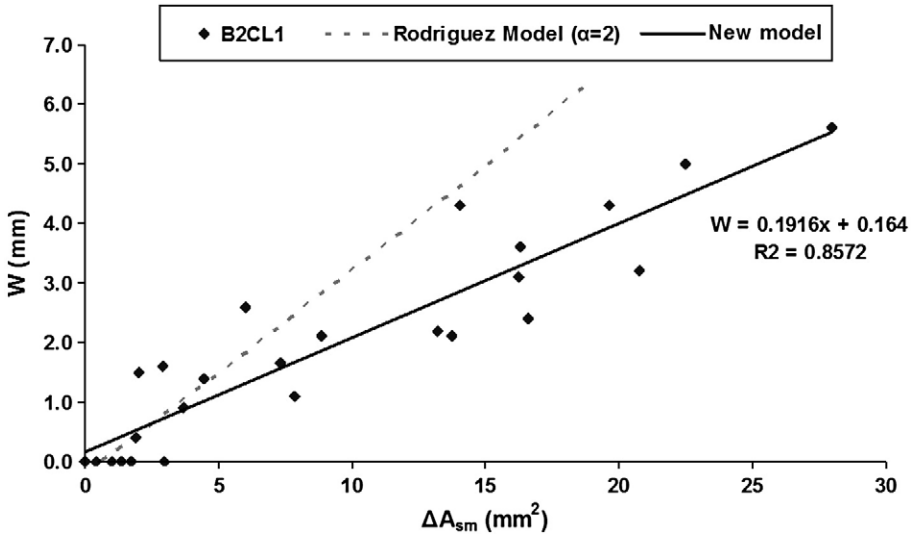

Fig. 16. Crack width evolution versus average cross-section loss of corroded beam B2CL1.

Generally, the corrosion pattern accelerated by imposing direct electrical current is closer to a general corrosion like the natural corrosion during the second stage of propagation. Even though Rodriguez's model derived from accelerated corrosion takes the corrosion pattern into account by the penetration parameter α, the comparison between models and experimental results illustrates that Rodriguez's model matches neither the localized corrosion pattern nor the general corrosion pattern of the natural chloride-induced corrosion process. Therefore, caution is required when the models derived from accelerated corrosion on small size specimens are used in large elements under natural corrosion. Further verification is necessary before the models can be validated on structures on site.

For a given corrosion crack, the prediction of localized cross-section loss based on Vidal et al.'s model is always higher than the average cross-section loss predicted by the new proposed model. Due to the complex corrosion distribution of the embedded rebar in an actual corroded structure, it is impossible to know in advance whether the given part of the structure is in the "localized corrosion phase" or "general corrosion phase". Therefore, in practice, both models can be used together to determine the minimal and the maximal limits of reinforcement corrosion level to assess the change in mechanical behaviour of the corroded structure. It should be noted that, under the general corrosion pattern, the prediction of Vidal et al.'s model may be too conservative.

References

[1] B. Elsener, Corrosion rate of steel in concrete — measurements beyond the Tafel law, Corrosion Science 47 (2005) 3019–3033.

[2] M.F. Montemor, A.M.P. Simões, M.G.S. Ferreira, Chloride-induced corrosion on reinforcing steel: from the fundamentals to the monitoring techniques, Cement & Concrete Composites 25 (2003) 491–502.

[3] C. Andrade, C. Alonso, On-site measurements of corrosion rate of reinforcements, Construction and Building Materials 15 (2001) 141–145.

[4] J. Rhazi, S. Laurens, G. Ballivy, Insights on the GPR non destructive testing method of bridge decks, Special Session on Non Destructive Detection of Corrosion in Reinforced Concrete, ACI Meeting, Toronto, 2000.

[5] C. Alonso, C. Andrade, J. Rodriguez, J.M. Diez, Factors controlling cracking of concrete affected by reinforcement corrosion, Materials and Structures 31 (1998) 435–441.

[6] J. Rodriguez, L.M. Ortega, J. Casal, J.M. Diez, Assessing structural conditions of concrete structures with corroded reinforcements, 4th Int. Congress on concrete in the service of mankind, Proceedings of an International Conference, Dundee UK, 1996.

[7] T. Vidal, A. Castel, R. François, Analyzing crack width to predict corrosion in reinforced concrete, Cement and Concrete Research 34 (2004) 165–174.

[8] F. Paradis, V. Lapointe, M. Jolin, J. Marchand, Accelerated test methods to investigate chloride-induced steel corrosion damage in reinforced concrete — a brief review, in: V.M. Malhotra (Ed.), Seventh CANMET/ACI International Conference on Durability of Concrete, Montreal, May 28–June 3 2006, pp. 357–373.

[9] R. François, G. Arliguie, Reinforced concrete: correlation between cracking and corrosion, Proc., 2nd CANMET/ACI Int. Conf. On Durability of Concrete, SP126, Montreal, Canada, 1991, pp. 1221–1238.

[10] A. Castel, R. François, G. Arliguie, Mechanical behavior of corroded reinforced concrete beams—Part 1: Experimental study of corroded beams, Materials and Structures 33 (Nov 2000) 539–544.

[11] A. Castel, R. François, G. Arliguie, Mechanical behavior of corroded reinforced concrete beams—Part 2: Bond and notch effects, Materials and Structures 33 (Nov 2000) 545–551.

[12] T. Vidal, A. Castel, R. François, Corrosion process and structural performance of a 17 year old reinforced concrete beam stored in chloride environment, Cement and Concrete Research 37 (2007) 1551–1561.

[13] T.A. Soylev, R. François, Corrosion of reinforcement in relation to presence of defects at the interface between steel and concrete, ACSE 17 (4) (2005).

[14] T.U. Mohammed, H. Hamada, Corrosion of horizontal bars in concrete and method to delay early corrosion, ACI Materials Journal 103 (5) (September–October, 2006).

[15] T.U. Mohammed, N. Otsuki, H. Hamada, Corrosion of steel bars in cracked concrete under marine environment, Journal of Materials in Civil Engineering, (ASCE) 0899-1561 (2003) 15:5(460).

[16] P. Schiessl, M. Raupach, Laboratory studies and calculations on the influence of crack width on chloride-induced corrosion in concrete, ACI Materials 94 (n°1) (1997).

[17] C.Q. Li, Corrosion initiation of reinforcing steel in concrete under natural salt spray and service loading — results and analysis, ACI Materials Journal 97 (6) (2002) 690–697.

[18] R. François, G. Arliguie, Effect of microcracking and cracking on the development of corrosion in reinforced concrete members, MCR (ISSN: 0024-9831) 51 (2) (1999) 143–150.

[19] G.K. Glass, N. Davision, A.C. Roberts, Pit realkalisation and its role in the electrochemical repair of reinforced concrete, Journal of Corrosion Science and Engineering 9 (2006) Paper no.10.

[20] O. Poupard, V. L'Hostis, S. Catinaud, I. Petre-Lazar, Corrosion damage diagnosis of a reinforced concrete beam after 40 years natural exposure in marine environment, Cement and Concrete Research 36 (2006) 504–520.